www.acsnano.org

Modulating Surface Structural Evolution of LiCoO₂ for Enhanced Extreme Fast-Charging Durability

Yuhao Du,[#] Wenguang Zhao,[#] Zijian Li, Hengyu Ren, Haocong Yi, Shengyu Wu, Jun Wang,* Feng Pan,* and Qinghe Zhao*



Downloaded via UNIV TOWN OF SHENZHEN on November 18, 2025 at 07:03:40 (UTC). See https://pubs.acs.org/sharingguidelines for options on how to legitimately share published articles.

Cite This: ACS Nano 2025, 19, 25951-25961



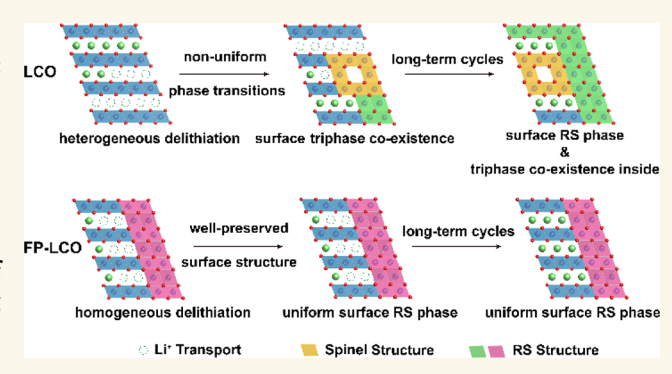
ACCESS I

Metrics & More

Article Recommendations

s Supporting Information

ABSTRACT: The applied cathodes in lithium-ion batteries usually suffer from severe structural degradation upon fast charging, and the correlated mechanism still remains vague. Here, we reveal the surface structural evolution of LiCoO₂ (LCO) during cycling at 4.6 V vs Li/Li⁺ with an extreme high fast-charging current of 10 C. Fast charging induces surface heterogeneous delithiation, promoting nonuniform surface phase transitions and resulting in the formation of a triphase hybrid on the charged surface. The triphase hybrid consists of the layered, spinel, and rock-salt (RS) phases. As cycling proceeds, this triphase hybrid propagates gradually toward the bulk, accompanied by a progressive thickening of the surface RS phase, leading to deteriorated Li⁺ transport kinetics and



accelerated capacity fading. Thus, suppressing the heterogeneous Li⁺ delithiation of LCO is crucial for enhancing fast-charging durability. By applying a uniform and robust surface coating, the surface delithiation homogeneity upon extreme fast charging is significantly improved, and the thickening of the surface Li⁺-blocking RS phase is greatly reduced, thereby achieving enhanced cycling stability of LCO. This work benefits the development of more advanced LCO cathodes tailored for fast-charging applications.

KEYWORDS: LiCoO₂, structure evolution, fast charging, cycle stability, rock-salt phase

INTRODUCTION

With the progressive depletion of fossil energy resources, research efforts have shifted toward alternative clean energy solutions, among which fuel cells and lithium-ion batteries serve as efficient energy carriers. Currently, the increasing demand for advanced Li-ion batteries (LIBs) in fields such as electric vehicles, consumer electronics, and energy storage systems has promoted the research, production, and application of advanced cathode materials. Among various cathode materials, LCO has been widely utilized owing to its outstanding volumetric energy density, long cycle life, and high operational voltage. Nowadays, to achieve higher energy density, the industry has sought to develop LCO/graphite full batteries with an upper cutoff voltage of 4.55 V, corresponding to 4.6 V vs Li/Li⁺ for the LCO cathode. Extensive research has been conducted to clarify the critical issues of high-voltage LCO cathodes, including irreversible phase evolution, capacity degradation, and cell performance optimization strategies.2

In addition to achieving high energy density, other performance metrics, such as high/low temperature capability and fast charging/discharging capability, are also essential in practical applications. Among these requirements, the demand for fast charging is particularly pressing because of the rapidly growing number of mobile electrical devices. The industry has attempted to make the charging time as short as possible, seeking a charging rates of 10 C or even higher. However, charging at such a high rates remains a significant challenge. Fast charging usually leads to accelerated structural degradation, the cycle life of the cathode compared to slow charging. 13,14

Received: April 9, 2025 Revised: July 1, 2025 Accepted: July 1, 2025 Published: July 12, 2025





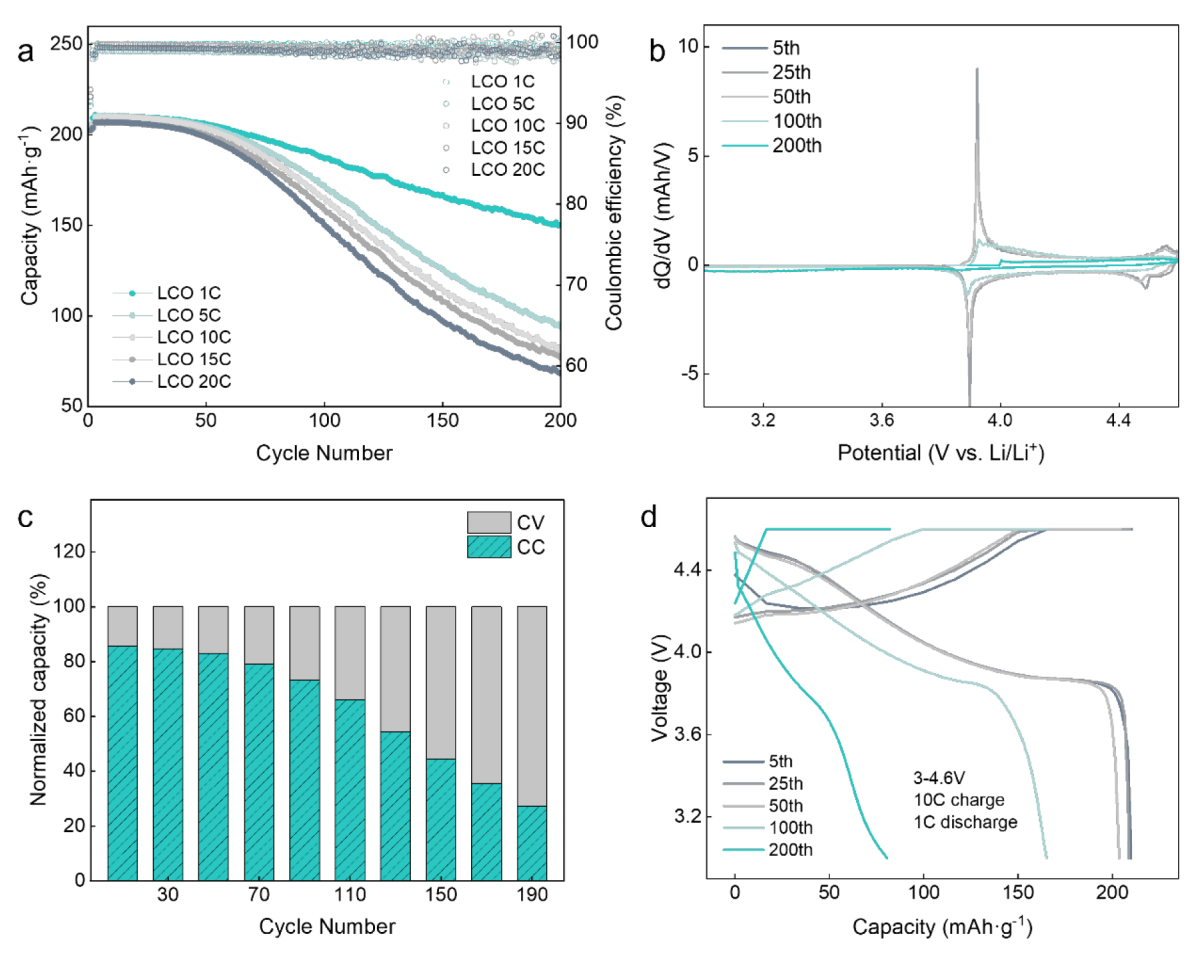


Figure 1. Electrochemical performance of LCO. (a) Cycle stability under different charging rates. (b) dQ/dV curves after different fast-charging cycles. (c) Contributions of CC and CV to the charging capacity during cycling. (d) Charge/discharge curves during different fast-charging cycles.

Nowadays, for fast-charging-induced issues, most research has focused on regulating the Li⁺ insertion behavior in graphite anodes and identifying it as the primary cause of failure during fast charging, mainly due to the poor Li⁺ transport kinetics in graphite-based anodes. 15,16 Multiple strategies have been proposed, including electrolyte engineering, 17-23 material optimization, 24,25 separator modification, 26 and applying new charging protocols. 27,28 However, research on cathode degradation induced by fast charging is still lacking. Current studies have revealed that fast charging can exacerbate both surface and bulk structural degradation, resulting in increased polarization and particle cracking. 29-32 The underlying reason is that fast charging tends to induce significant chemical heterogeneity within the cathodes and among the cathode particles across the entire electrode. Additionally, it accelerates electrolyte decomposition. These issues can be partially mitigated by surface modification, 38,39 element doping,40,41 and electrode structure optimization, 42,43 etc. Although the above research has revealed the adverse effects of fast charging, it has not fully clarified how structural degradation evolves or how these strategies alleviate fastcharging-induced degradation.

In this work, we not only investigate the surface structural evolution of LCO upon fast charging at 10 C but also propose an effective surface coating strategy to suppress structural degradation effects. As illustrated, surface heterogeneity poses significantly deteriorates for LCO cathode cycling during fast

charging. For LCO, a triphase hybrid is observed on the surface after the first 10 C charging, mainly attributed to nonuniform Li⁺ delithiation. In this surface triphase hybrid, significant differences among these phases lead to considerable localized internal stress accumulation, which triggers the migration and loss of active lattice O^{n-} (0 < n < 2) and causes the transition from a layered to a pure RS phase upon cycling. As cycling proceeds, this triphase hybrid gradually propagates from the surface into the bulk, accompanied by a continuous increase in the thickness of the surface RS phase. Since the RS phase usually exhibits poor Li⁺ ion conductivity, its progressive thickening upon cycling directly causes the rapid deterioration of Li+ transport kinetics, leading to rapid capacity decay. Collectively, we recognize that homogenizing surface Li+ delithiation is behavior is crucial to enhancing the fast-charging durability of LCO. This work further proposes an F/P-based surface coating of LCO (namely, FP-LCO) to improve delithiation uniformity across the LCO surface, thereby reducing the formation of the surface RS phase and improving the stability of the FP-LCO cathode during fast charging. As a result, the FP-LCO/Li cell exhibits an impressive retention of 91.6% after 200 cycles (charged at 10 C and discharged at 1 C), which is much superior to that of the LCO/Li cell (38.3% over 200 cycles).

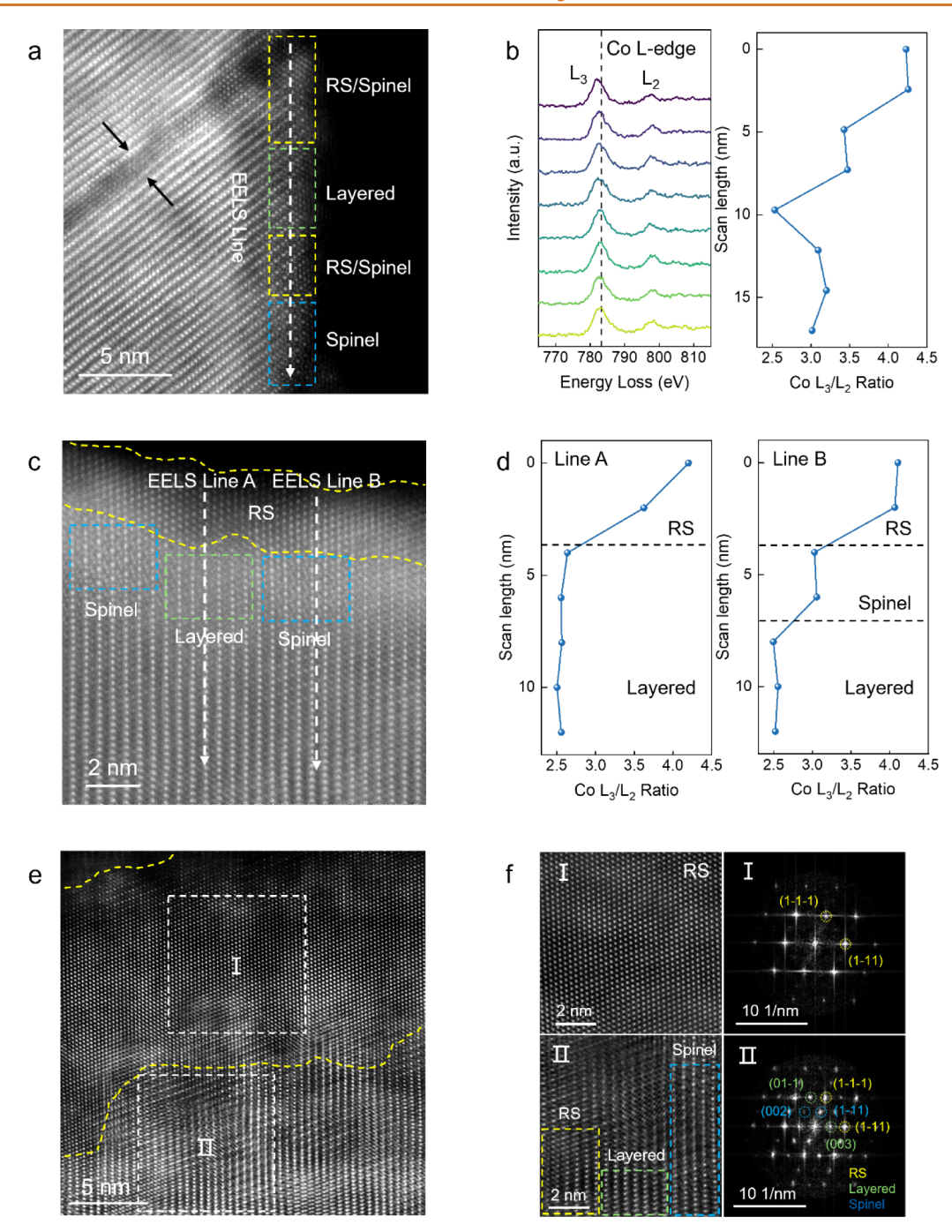


Figure 2. Surface structural characterization of LCO after the 25th, 100th, and 200th fast-charging cycles. (a) Surface structure and (b) Co L_3/L_2 ratio results after 25 cycles. (c) Surface structure and (d) EELS analysis results after 100 cycles. (e) Surface structure and (f) FFT analysis results after 200 cycles.

RESULTS AND DISCUSSION

Rapid Capacity Fading of LCO upon Fast Charging. To investigate the structural evolution of LCO degradation upon fast charging, a commercial LCO was employed, with Dco

upon fast charging, a commercial LCO was employed, with D_{50} of about 5 μ m and is doped with 4500 ppm of Al. The morphology of LCO is presented in Figure S1. Coin-type LCO/Li cells were assembled and tested upon fast charging. The detailed cell test protocol is as follows: first, the cell is charged to 4.6 V with various constant currents (CC stage), including currents of 1 C, 5 C, and 10 C, etc. (1 C = 0.2 A·g⁻¹), followed by constant voltage (CV) charging until reaching a cutoff current of 0.2 C. Subsequently, the cell was

discharged with a constant current of 1 C. Compared to CC charging, CC + CV charging can release more Li⁺ ions from LCO, making it widely applied in practical applications.

The comparison of cycle performance of LCO/Li cells under different fast charging rates is presented in Figure 1a. As observed, when the CC charging current increased from 1 to 20 C, the discharge capacity remained nearly unchanged, whereas the cycle stability of LCO/Li cells gradually declined. After 200 cycles, the capacity retention of the LCO/Li cell charged at 1 C was 70.9%, significantly higher than that charged at 10 C (38.3%), indicating the markedly reduced cycling stability during fast charging. As previously reported,

applying CC + CV charging can accelerate the capacity decay of LCO due to aggravated surface reactions.⁴⁴ Therefore, simultaneous application of CC + CV and fast charging will inevitably lead to accelerated capacity decay. Elucidating the degradation mechanism during fast charging will provide valuable guidance for practical applications.

For LCO/Li cells charged at 10 C, the dQ/dV curves were obtained to illustrate the electrode behavior of LCO at the 5th, 25th, 50th, 100th, and 200th cycles, as shown in Figure 1b. The dQ/dV curves are derived from the charge/discharge curves at 0.2 C after the selected cycles, and the selected data points are presented in Figure S2. At the 100th cycle, no redox peaks were observed, suggesting severely suppressed phase transitions in LCO. In addition to the dQ/dV curve, we also extracted the contributions of CC and CV stages to the charging capacity during cycling from the 0.2 C chargedischarge curves, as shown in Figure 1c. As the cycle number advances beyond the 100th cycle, the proportion of CV stage charging increases rapidly. This result may indicate that once the surface structure of LCO deteriorates, the Li⁺ transport channels will be quickly blocked, which in turn requires a longer CV charging time at 4.6 V to reach the fully charged status, thereby further deteriorating the surface structure of LCO. As a result, the above processes ultimately lead to the initiation and perpetuation of undesirable surface side reactions, resulting in the rapid capacity decay of the LCO/

In addition, as observed in Figure 1d, after the 100th cycle, the LCO/Li cell exhibited significant polarization during the charge/discharge processes, indicating severe surface degradation of LCO. Thus, we further perform electrochemical impedance spectroscopy (EIS) and galvanostatic intermittent titration technique (GITT) to examine the changes in impedance and the diffusion coefficient (D_{Li}^+) . The EIS plots are shown in FigureS3. By fitting the EIS plots, two important parameters are obtained, i.e., the impedance of the surface film or the cathode electrolyte interface (CEI) (R_t) , and the impedance for the charge transfer through the surface of LCO $(R_{ct})^{45}$ As observed, the value of R_f shows a slight change, while the value of R_{ct} shows a significant increase in 200 cycles. Compared to the diffusion coefficient (D_{Li^+}) of LCO at the 25th cycle, the $D_{\mathrm{Li}^{+}}$ significantly decreased by the 200th cycle, as shown in Figure S4.

As discussed above, applying fast charging significantly accelerates surface structural degradation of LCO, leading to increased cell polarization, elevated interface impedance, and a rapid decline in $D_{\rm Li^+}$ across the LCO surface. These factors collectively contribute to the rapid capacity fading of LCO/Li cells. Investigating the degradation mechanism of the LCO surface is crucial for designing advanced LCO cathodes with reinforced fast-charging durability, which will be discussed in detail in subsequent sections.

Surface Evolution of LCO upon Fast Charging. As discussed above, surface structural degradation is regarded as the root cause of the rapid capacity decay of LCO upon fast charging. To further reveal the structural evolution of LCO, transmission electron microscopy (TEM) and correlative electron energy loss spectroscopy (EELS) analyses were performed. For LCO, it exhibits a pure layered bulk structure (Figure S5). However, in the surface region, some localized structural heterogeneity inevitably exists due to exposure to CO_2 and H_2O in air. This type of structural heterogeneity leads

to certain differences in Li⁺ transport kinetics, resulting in faster Li⁺ transport in some localized surface regions and slower Li⁺ transport in others. The influence of such subtle differences on the cycling stability of LCO is negligible at slow-charging rates, such as 0.5 C. However, when the charging rates increases to 10 C, it significantly exacerbates the heterogeneity of Li⁺ delithiation on the LCO surface. This heterogeneous delithiation directly leads to the nonuniform Li⁺ distribution on the LCO surface. As a result, upon charging, some regions with higher residual Li⁺ ions retain the pristine layered structure, while other regions with excessive Li⁺ extraction transform into nonlayered phases, including spinel or RS phases.

As shown in Figure 2a, at the 25th cycle, some regions of the LCO surface (regions with lower Li⁺ retained) preferentially evolve into spinel or RS phases driven by Co dissolution and oxygen release, while other regions (with higher residual Li⁺ ions) still retain the layered structure, accompanied by the formation of minor cracks. Thus, upon fast charging, the surface structure transforms from a layered phase to a triphase hybrid, which becomes strikingly evident by the 25th cycle. Figure S6 presents surface structural images from another region, further demonstrating the ubiquity of the triphase hybrid on the surface of LCO.

We further performed electron energy loss spectroscopy (EELS) to analyze the triphase coexistence on the LCO surface, as shown in Figures 2b and S7. The changes in the Co L_3 edge-peak and the intensity ratio of Co L_3/L_2 peaks on the LCO surface after 25 cycles of fast charging are presented. As observed, along the surface region from 0 to 17 nm, the phase structure sequentially transitions from spinel, RS/spinel mixed, layered, and then to the RS phase, accompanied by shifts in the Co L3-edge peaks, as well as significant fluctuations in the intensity ratio of Co L₃/L₂ peaks. Specifically, the intensity ratios of Co L_3/L_2 peaks for the RS, spinel, and layered phases are about 4.0, 3.0, and 2.5, respectively. Additionally, changes in the O K-edge prepeak intensity also reflect variations in the surface phase structure. The prepeak intensity first weakens, then increases, and finally weakens again along the scanning path, which is consistent with the variations observed in the Co L₃ edge results. As noted, at the 25th cycle, although the triphase coexistence appears on the surface, its thickness is relatively small (less than 3 nm), and the bulk phase maintains a well-preserved layered structure. Thus, the capacity degradation of LCO is not significant at this stage.

Due to heterogeneous delithiation, a triphase coexistence forms on the LCO surface at the 25th cycle. This triphase coexistence further increases the heterogeneity of surface chemical states, thereby exacerbating the nonuniform Li⁺ delithiation from the surface during fast charging. As cycling proceeds, the degradation of the surface structure accelerates. As shown in Figure 1a, capacity is severely degraded after the 100th cycle. Thus, we selected the LCO electrode at the 100th cycle and analyzed its surface structure using TEM and EELS. In Figure 2c, at the 100th cycle, the surface triphase coexistence observed at 25 cycles has fully evolved into the RS phase with a thickness of 3 nm. Beneath this RS layer, a new triphase coexistence region is formed with alternating distributions of the layered, spinel, and RS phases. Figure S8 also presents the surface structural images of another region, further demonstrating the ubiquity of triphase coexistence in the subsurface of LCO. The possible mechanism for the above surface structural evolution is as follows: within the surface

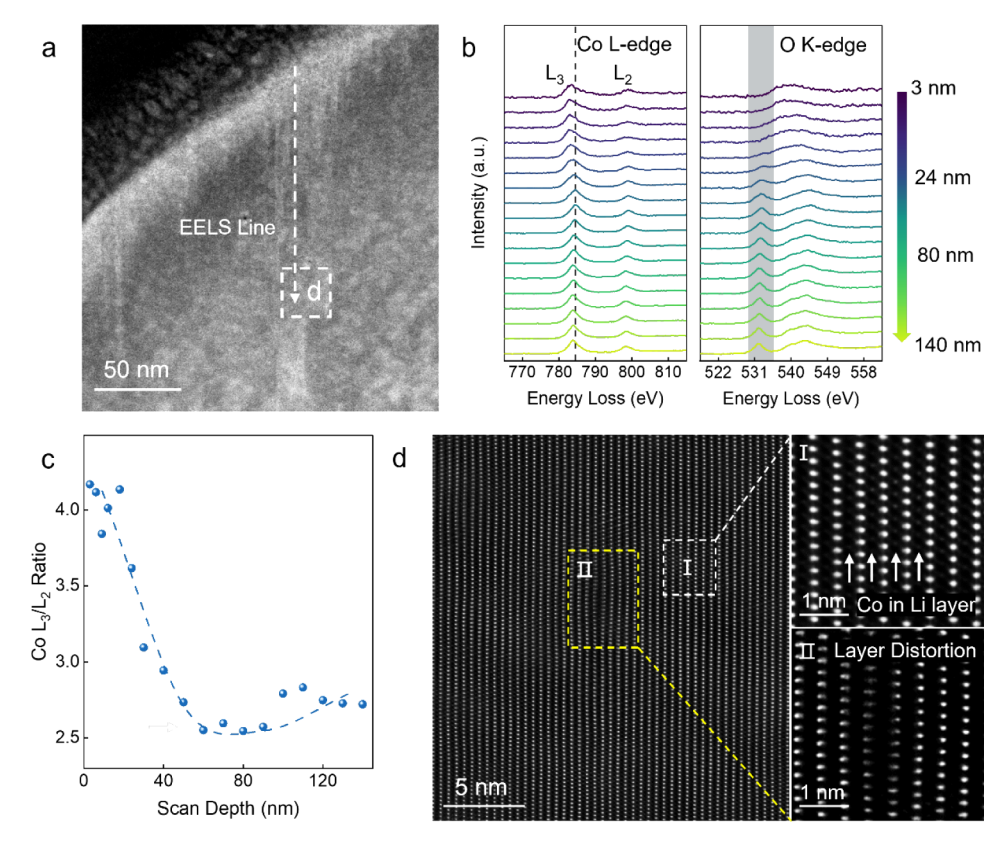


Figure 3. Further characterization results of LCO after 200 cycles. (a) EELS scan path from the surface to the bulk and (b) the corresponding analysis results. (c) Co L_3/L_2 ratio results. (d) Characterization results of the bulk structure.

triphase coexistence region at the 25th cycle, the spinel and layered phases exhibit higher Li⁺ transport kineticsthan the RS phase. Thus, upon fast charging, more Li⁺ ions are delithiated from the surface spinel and layered phases rather than the RS phase, ultimately driving transformation from the layered/spinel phases into the RS phase. As a result, the initial triphase coexistence on the surface inevitably evolves into a pure RS phase after 100 cycles. Besides, despite the formation of a thin surface RS phase, it is unable to prevent uneven delithiation, and similar structural evolution observed at the 25th cycle will further occur beneath this RS phase layer, where the layered structure evolves into a phase coexistence structure.

Similarly, as shown in Figure 2c, two scanning paths, line A and line B, were selected for EELS analyses. As shown in Figure S9, along line A, the shift of Co L-edge L₃ peaks diminishes at a depth of around 4 nm, indicating the direct transition from RS to layered phases. Conversely, along line B, the shift of Co L-edge L₃ peaks diminishes at a depth of around 6 nm, indicating the transitions from RS to spinel phases and then to layered phases. Figure 2d displays the variation in the Co L_3/L_2 peak ratio values along scan lines A and B, respectively. It is clearly observed that the changes in the Co valence state along scan lines A and B correspond well to the structural evolution from the surface to the bulk, and they also demonstrate the thin RS-phase layer on the outermost surface and the triphase coexistence in the subsurface region. In Figure \$10, we also performed a comparison of the O K-edge, and the results are consistent with those of the Co L-edge. The EELS results further confirm the structure observed in Figure 2c, where the surface consists of an RS layer and the subsurface a triphase coexistence region. At the 100th cycle, on one hand, the RS layer, which evolves from structural degradation,

continuously thickens, leading to an increase in the polarization of LCO (Figure 1d), making the Li⁺ delithiation process more difficult and thereby causing capacity degradation. On the other hand, the subsurface triphase coexistence region continues to propagate toward the bulk. As a result, the subsurface of LCO still exhibits nonuniform delithiation upon fast charging, and the structural evolution from the triphase coexistence to the RS phase persists on the surface, leading to the continuous thickening of the surface RS phase (acting as a Li⁺ blocking phase) and accelerating rapid capacity degradation

In Figure 1a, we observed that the capacity of LCO is reduced to around 70 mA h g⁻¹ by the 200th cycle, indicating the failure of the LCO cathode. Therefore, we selected the LCO at the 200th cycle to demonstrate the fully deteriorated surface structure. In Figure 2e, the surface structure continuously evolves and degrades, resulting in the formation of the surface RS phase with a thickness of about 20 nm. Beneath this RS phase layer, triphase coexistence still remains. We selected two regions (I and II) within the RS layer and the triphase coexistence region for magnification, as shown in Figure 2f. It is observed that region I exhibits a pure RS phase, and region II shows a triphase coexistence with more disordered character compared to those at the 25th and 100th cycles. Additionally, EELS analyses cannot provide clear results in this region, so we perform fast Fourier transform (FFT) analyses to further confirm the presence of this triphase coexistence. As shown in Figure 2f, diffraction spots corresponding to each phase are clearly marked, confirming the coexistence of the layered, spinel, and RS phases.

The surface structural evolution observed after 200 cycles is generally consistent with previous stages, showing continuous

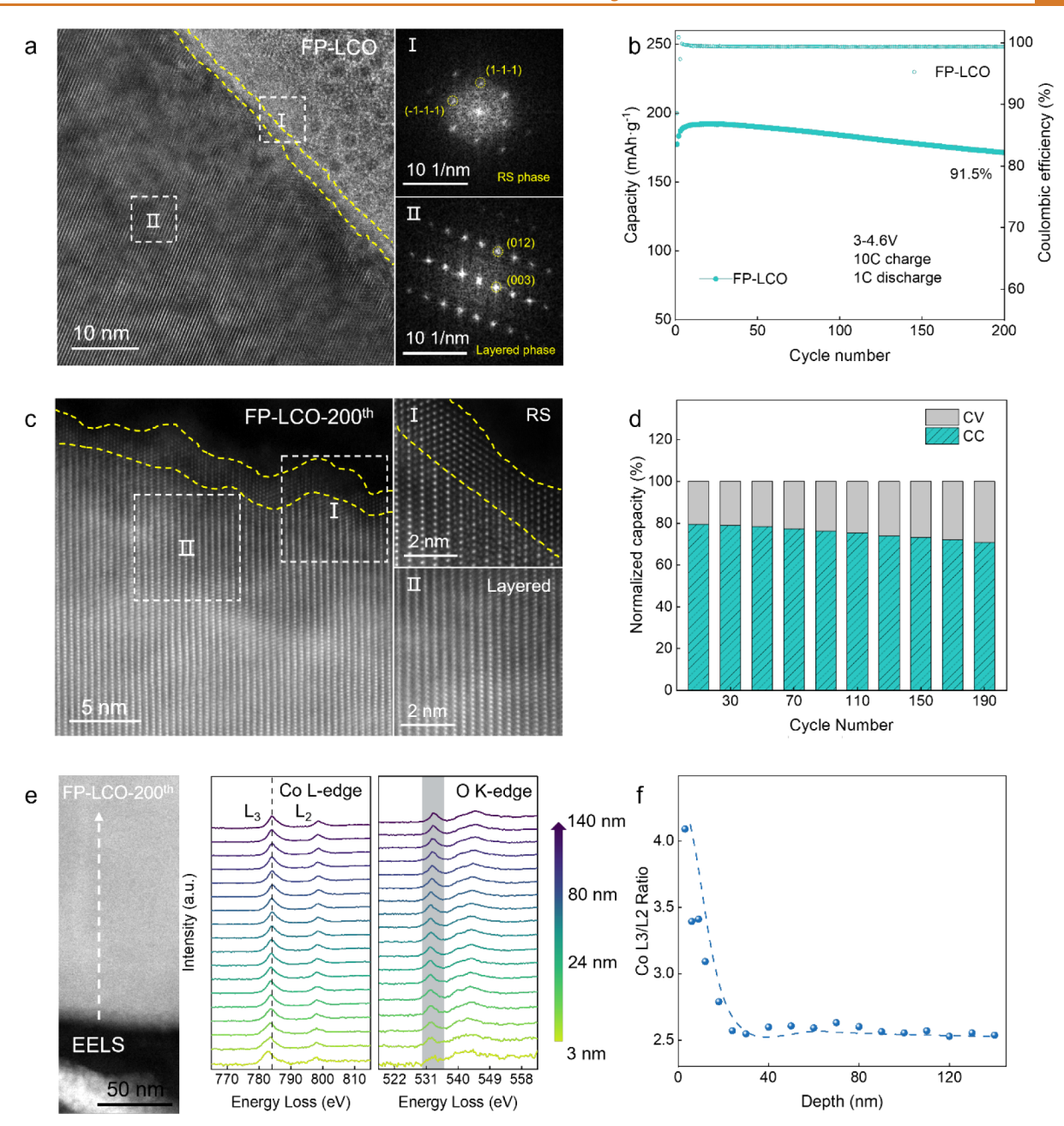


Figure 4. Comprehensive characterization results of FP-LCO before and after fast-charging cycles. (a) Characterization results of the pristine surface structure. (b) Cycle stability during 10 C fast-charging cycles. (c) Surface structural characterization results after 200 cycles. (d) Contributions of CC and CV to the charging capacity. (e) EELS scan path from the surface to the bulk and the corresponding analysis results. (f) Co L_3/L_2 ratio results.

evolution and migration of triphase coexistence regions. Additionally, as shown in Figure S11, numerous cracks are observed near the surface of LCO. We hypothesize that these cracks result from the accumulation of internal stresses. In Figure S12, a geometric phase analysis (GPA) is performed on the surface region (Figure 2e), revealing significant stress accumulation, which confirms our hypothesis. Moreover, we speculate that the disordered triphase coexistence region at the 200th cycle is also influenced by these cracks, which provide pathways for electrolyte infiltration and subsequent side reactions. The electrolyte infiltration into the subsurface triphase coexistence region, leading to a chaotic distribution of deteriorated phases. Furthermore, structural analyses on the surface of LCO subjected to slow-charging cycles are

performed (at a current of 1 C, at the 25th cycle, Figure S13). The results show that the triphase coexistence regions on the surface of LCO only occur during fast-charging cycles, rather than during slow-charging cycles.

To gain a more comprehensive understanding of the abovesurface structural evolution of LCO, we perform a large-scale EELS analysis in a range beyond 100 nm, with the scanning paths marked in Figure 3a. The L3 peaks of the Co L-edge exhibit significant shifts, and the prepeaks of the K-edge disappear within the surface region of 24 nm, corresponding to the thick surface RS layer and the triphase coexistence region beneath it (Figure 3b). Additionally, the L3 peaks of the Co Ledge show shifts within the surface region of 80–140 nm. These shifts are more clearly represented in the Co L₃/L₂

spectra (Figure 3c). These results indicates that applying fast charging has a subtle impact on the bulk structure of LCO. Thus, we select a region of the bulk phase (a specific location in Figure 3a) to further examine the bulk structural evolution. In Figure 3d, the bulk phase of LCO remains intact, with no significant structural damage. However, minor structural issues are observed in some localized regions. In region I, some Co atoms are found to migrate into the Li layer, while in region II, there is slight distortion in the bulk lattice. These results indicate that surface inhomogeneous delithiation can induce minor structural damage to the bulk, including Co migration and distortion of Co-O layers. However, from a macroperspective, the bulk phase maintains a relatively wellpreserved layered structure, as shown in Figure S14. In addition, SEM was employed to detect particle-level characterizations (Figures S15 and S16). Even after 200 cycles, no obvious cracks are observed. Thus, based on the above, the rapid capacity degradation of LCO induced by fast charging is caused mainly by surface deterioration rather than the bulk; moreover, such structural degradation is only confined to the surface region within 100 nm and rarely affects the bulk portion of the LCO cathode.

Surface Homogenizing to Reduce the Fast-Charging-**Induced Structure Degradation.** As discussed above, the rapid capacity degradation of LCO upon fast charging originates from surface structural evolution triggered by nonuniform Li⁺ delithiation. Thus, to alleviate this type of capacity decay, robust and uniform surface modification is essential. Based on this point, we developed a F/P dual optimization strategy to homogenize the LCO surface, and the coated LCO is labeled as FP-LCO. The synthesis of FP-LCO is as follows: the LCO was first mixed with nanosized LiF and Li₃PO₄ powders via ball milling; then, the obtained mixture was annealed at 700 °C for 5 h in an Ar atmosphere. The obtained FP-LCO is characterized via SEM and energydispersive spectrometry (EDS) (Figure S17), demonstrating successful F/P coating on the LCO surface. As shown in Figure S18, X-ray photoelectron spectroscopy (XPS) results clearly reveal that surface F exists as LiF and CoF2 species, corresponding to binding energies of ~685.1 eV and ~686 eV, respectively, and the surface P exists in the form of Li₃PO₄, similar to that reported in the work of Bi et al., corresponding to the binding energy of \sim 133.5 eV. 38,46

Besides the F/P coating, the surface structure is also reinforced. Figure 4a shows the cross-sectional characterization of the FP-LCO surface via TEM. As observed, there exists a thin surface RS layer, which is confirmed by the FFT result and is compact and uniform, with a thickness of about 2 nm (region I). Beneath this RS layer, we observe the pure layered structure in the bulk (region II). Furthermore, the F/P coating does not significantly alter the bulk structure, as revealed by X-ray diffraction (XRD) (Figure S19). In previous reports, the prefabricated surface RS layer benefits a lot in suppressing the detrimental side reactions derived from the highly oxidative $\text{Co}^{4+}/\text{O}^{\alpha-}$ (0< α < 2), thus leading to enhanced cycle stability. 9,47,48 Moreover, compared with the layered phase, the structural heterogeneity of the surface RS phase can also be largely reduced, thus benefiting the inhibition of surface deterioration of LCO during fast charging.

As expected, the FP-LCO/Li cell exhibits an impressive capacity retention of 91.6% after 200 cycles (charged at 10 C and discharged at 1 C), which is significantly better than that of the LCO/Li cell (38.3% in 200 cycles; Figure 4b). Figure

S20 provides comparative analyses of capacity retention versus cycle number for LCO and FP-LCO cathodes, demonstrating the superior cycling stability of FP-LCO. Meanwhile, Table S1 compares our results with previous studies, showing the competitive cell performance of the FP-LCO cathode. Correspondingly, the charge/discharge curves of the FP-LCO/Li cell maintain low polarization even up to 200 cycles (Figure S21), and the dQ/dV curves demonstrate highly reversible redox reactions over 200 cycles (Figure S22), which are much superior to those of the LCO/Li cell. SEM results after cycling (Figure S23) show that the cycled FP-LCO particles remain intact, with no visible structural damage. TEM was further applied to reveal the surface structure of FP-LCO after 200 cycles (Figure 4c). As observed, a thin surface RS layer is present on the surface of FP-LCO, with a thickness of about 2 nm. Beneath this RS layer, the layered structure is wellmaintained. The results illustrate that surface homogenization can significantly stabilize the surface structure of FP-LCO during fast charging and effectively suppress capacity decay. In other words, surface homogenization is an effective approach to prevent the structural evolution of the LCO surface caused by fast charging.

Figure 4d further shows the variations in the charging capacity proportion during the CC and CV stages. The results indicate that the charging capacity contributed by the CC stage of the FP-LCO/Li cell decreases slightly over cycles, which is very different from that of the LCO/Li cell (Figure 1d), indicating that the surface F/P-based homogenization can facilitate the Li⁺ transport even after 200 cycles. For FP-LCO at the 200th cycle, EELS analysis was applied to detect the Co valence states from the surface to the bulk (Figure 4e). Unlike the LCO at the 200th cycle (Figure 3c), the Co L₃ peaks of the Co L-edge show a slight shift within the surface region of 24-140 nm, and the Co L₃/L₂ ratio varies slightly in this region (Figure 4f), indicating a stabilized layered structure from the near-surface to bulk. XRD analysis was performed on both LCO and FP-LCO cathodes after 200 cycles, comparing their (003) peaks (Figure S24). The (003) peaks of both cathodes exhibit sharp, symmetric profiles, indicating well-preserved bulk structural integrity after cycling. Crucially, a peak shift is observed for LCO relative to FP-LCO, indicating mild interlayer distortion and enlarged interlayer spacing in cycled LCO. These XRD findings align with Co valence state analyses, collectively confirming the superior structural stability of FP-LCO in long-term cycles. In this work, although surface homogenization enhances structural stability, a slight reduction in discharge capacity is observed. Thus, a balance between enhancing stability and maintaining high capacity release must be considered in the future.

To gain a deeper understanding, we conducted further electrochemical tests on FP-LCO and compared them with LCO. As shown in Figure S25, the EIS results of both cathodes are compared, revealing a significant difference in the $R_{\rm ct}$ values during cycling. FP-LCO shows a much smaller increase in the value of $R_{\rm ct}$ compared with LCO, which is attributed to the suppression of surface structural evolution. The GITT results presented in Figure S26 also lead to the same conclusion, where the $D_{\rm Li}$ value of FP-LCO remains almost unchanged during cycling, indicating a stable surface structure. Notably, in the EIS results, the $R_{\rm f}$ values for both materials show no significant difference. This value typically reflects the CEI on the cathode surface, so we characterize the CEI for both materials. As shown in Figure S27, the CEI on the surfaces of

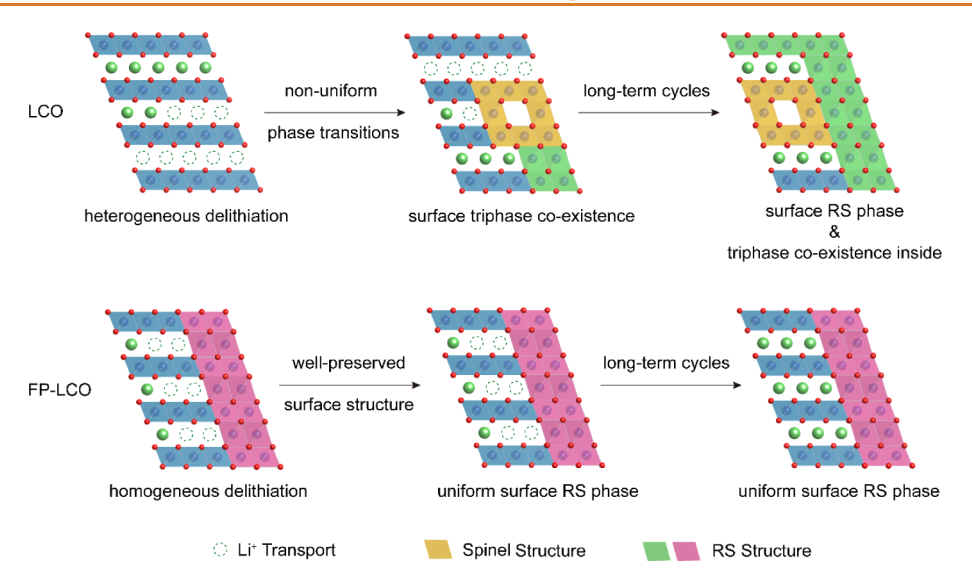


Figure 5. Schematic illustrations of the surface structural evolution of LCO and FP-LCO cathodes upon fast charging. While LCO surfaces degrade from layered \rightarrow triphase hybrid \rightarrow RS + triphase hybrid upon fast charging, the prefabricated RS layer on the surface of FP-LCO enables the uniform delithiation, enhancing the surface stability.

the two cathodes shows nearly identical characteristics, which is consistent with the EIS results. We analyzed the composition of the CEI. In Figure S28, both CEI layers contain a significant proportion of organic components. Furthermore, neither cathode exhibits a morphologically stable CEI. These results suggest that, without specific CEI modulation, efficient CEI formation under fast-charging conditions remains challenging. Furthermore, we performed temperature-dependent EIS tests to obtain energy barrier information for both materials (Figure \$29). The surface energy barrier of FP-LCO is significantly higher than that of LCO, primarily due to differences in their initial surface structures. Meanwhile, no Co signal was detected on the anode side for either anode (Figure S30), indicating that both anodes remain in similar chemical environments after cycling. Based on the above, we recognize that the cycle stability upon fast charging is not significantly correlated with the properties of the CEI but lies in the homogeneity and toughness of the surface structure, and the artificially homogenized and reinforced surface structure can effectively enhance the cycling stability of LCO upon fast charging. It is noted that this study focuses on fast-charging performances under high voltage (4.6 V), in which the highly delithiated state of cathodes can trigger the irreversible O3 to H1-3 phase transition, leading to significant structural degradation. In contrast, fast charging at lower voltages (e.g., 4.5 V, Figure S31) exhibits significantly better capacity retention due to the absence of such irreversible phase transitions.

Based on the above discussions, schematic illustrations of the surface structural evolution of LCO and FP-LCO cathodes upon fast charging are shown in Figure 5. For LCO, localized surface chemical states inevitably exhibit some degree of heterogeneity, leading to variations in the energy barriers for Li⁺ delithiation, which promote the formation of a triphase hybrid (including layered, spinel, and RS phases) on the surface of LCO upon fast charging. The emergence of the triphase hybrid further exacerbates the heterogeneity of Li⁺ delithiation on the LCO surface, causing stress accumulates within the surface zone and contributing to formation of the surface RS phase (shown in green). As the fast-charging cycle proceeds, surface structural degradation leads to the con-

tinuous thickening of the surface RS phase, which acts as an effective Li+ blocking layer and severely inhibits the Li+ delithiation at the surface, thereby causing rapid capacity degradation. To suppress capacity decay caused by heterogeneous surface delithiation, it is essential to homogenize the surface structure. In this work, the surface of FP-LCO is modified with F/P species, including fluoride and phosphate, along with a prefabricated surface RS phase (shown in orange). This surface modification effectively homogenize surface chemical states, leading to more uniform Li+ deintercalation upon fast charging. Attributed to the more homogeneous delithiation enabled by the FP-LCO cathode, the surface structure remains well-preserved even after long-term cycling. The thickness of the surface RS phase remains nearly unchanged, with well-retained Li⁺ transport kinetics, thereby improving capacity retention.

CONCLUSION

In summary, this work not only reveals the surface structural evolution of LCO during fast charging but also proposes an effective homogenization strategy to suppress structural degradation and improve fast-charging durability. Comprehensive characterizations, including SEM, TEM, XRD, XPS, EELS, and GPA, are employed to clarify the surface structural evolution of LCO and the correlated optimization mechanism. Nonuniform Li+ delithiation is the fundamental cause of the rapid capacity degradation of LCO upon fast charging, leading to the emergence of the triphase hybrid as well as the continuously thickening surface RS phase. It is noted that fastcharging-induced capacity fading is primarily related to surface structure rather than the bulk phase or the properties of CEI. Therefore, homogenizing the surface structure can effectively suppress surface deterioration and capacity decay. This work benefits the structural design of layered cathodes applied under fast-charging conditions.

EXPERIMENTAL SECTION

Sample Preparation. The commercial LCO powders were purchased from Pulead Technology Industry Co., Ltd. The FP-LCO was obtained by an F/P dual optimization strategy. The

synthesis process is as follows: 5 g of LCO, 0.014 g of LiF (99%, Aladdin), and 0.011 g Li $_3$ PO $_4$ (99%, Aladdin) were first mixed via manual grinding. During this process, anhydrous ethanol was added and continuously mixed until complete evaporation to ensure homogeneous blending of the materials, and then the mixture was annealed at 700 °C for 5 h in an Ar atmosphere.

Material Characterization. A scanning electron microscope (SEM, Zeiss SUPRA-55) with an X-Max EDS detector was used to obtain the morphology and elemental distribution of the samples. The transmission electron microscopy (TEM) analysis was conducted on a field-emission transmission electron microscope (FETEM, JEOL-3200FS) operating at an accelerating voltage of 300 kV, with a 60 cm camera length, a minimum collection angle of -30° to 30° , and a OneView CMOS camera (Gatan Inc.). The atomically resolved highangle annular dark-field scanning transmission electron microscopy (HAADF-STEM) images were acquired using an aberration-corrected scanning transmission electron microscope (FEI Titan Themis, operated at 300 kV). The obtained results were analyzed using the Digital Micrograph software to perform geometric phase analyses (GPA). TEM samples were prepared using a focused ion beam (FIB). A Thermo Scientific Escalab 250Xi spectrometer was used to obtain the X-ray photoelectron spectroscopy (XPS) results, confirming the chemical states of the selected elements. A Bruker D8 Advance diffractometer with a Cu K α radiation source ($\lambda = 0.154$ nm) was used to obtain the powder X-ray diffraction (XRD) data, and the Rietveld refinements of XRD patterns were performed with the FULLPROF suite.

Electrochemical Characterization. The electrode were prepared by stirring 80 wt % LCO, 10 wt % acetylene black, and 10 wt % polyvinylidene fluoride (PVDF) in N-methyl-2pyrrolidone (NMP) solvent and then drying at 80 °C for 1 h. After drying, the pieces were cut and dried at 105 °C under vacuum for 6 h. The final active material loading of the electrode pieces is about 6 mg cm⁻². The electrochemical performance was assessed by coin-type (CR2032) half-cells using lithium metal as the anode, a Celgard 2400 polypropylene (PP) membrane as the separator, and 1.0 M LiPF₆ in fluoroethylene carbonate/ethyl methyl carbonate/ fluoroethylene carbonate (FEC:EMC:FEC = 1:1:1 in vol %) as the electrolyte. CR2032-type coin cells were assembled by stacking: negative can, stainless steel spring spacer, polypropylene gasket, Li metal anode (1.5 mm thick), Celgard 2400 separator, cathode, and positive can. A total of 60 μ L of the electrolyte was injected. The charge and discharge tests and galvanostatic intermittent titration technique (GITT) tests were performed on a NEWARE battery test system at 25 °C. EIS was conducted on a Solartron Analytical 1470E electrochemical workstation.

ASSOCIATED CONTENT

Supporting Information

The Supporting Information is available free of charge at https://pubs.acs.org/doi/10.1021/acsnano.5c05981.

Characterizations of materials such as SEM, XRD, TEM, EELS, EDS, and XPS; electrochemical characterizations such as charge/discharge curves, GITT, dQ/dV curves and EIS; SEM morphology of LCO and FP-LCO; EIS and GITT results of LCO and FP-LCO at different cycles; charge/discharge and dQ/dV curves of FP-LCO;

TEM results of LCO and FP-LCO at different cycles; EELS analyses of LCO at 100th cycles and FP-LCO at 200th cycles; EDS and XPS results of FP-LCO; XRD results of LCO and FP-LCO (PDF)

AUTHOR INFORMATION

Corresponding Authors

Jun Wang — School of Innovation and Entrepreneurship, Southern University of Science and Technology, Shenzhen 518055, China; Email: wangj@sustech.edu.cn

Feng Pan — School of Advanced Materials, Peking University Shenzhen Graduate School, Shenzhen 518055, China; orcid.org/0000-0002-8216-1339; Email: panfeng@pkusz.edu.cn

Qinghe Zhao — College of Physics and Energy, Fujian Normal University, Fuzhou 350117, China; Email: katong880109@ 163.com

Authors

Yuhao Du - School of Advanced Materials, Peking University Shenzhen Graduate School, Shenzhen 518055, China

Wenguang Zhao — School of Advanced Materials, Peking University Shenzhen Graduate School, Shenzhen 518055, China

Zijian Li – School of Advanced Materials, Peking University Shenzhen Graduate School, Shenzhen 518055, China

Hengyu Ren – School of Advanced Materials, Peking University Shenzhen Graduate School, Shenzhen 518055, China

Haocong Yi – School of Advanced Materials, Peking
University Shenzhen Graduate School, Shenzhen 518055,
China

Shengyu Wu — College of Physics and Energy, Fujian Normal University, Fuzhou 350117, China

Complete contact information is available at: https://pubs.acs.org/10.1021/acsnano.5c05981

Author Contributions

[#]Y.D. and W.Z. contributed equally to this work.

Notes

The authors declare no competing financial interest.

ACKNOWLEDGMENTS

This work is financially supported by the Basic and Applied Basic Research Foundation of Guangdong Province (No. 2021B1515130002), the International Joint Research Center for Electric Vehicle Power Battery and Materials (No. 2015B01015), the Guangdong Key Laboratory of Design and Calculation of New Energy Materials (No. 2017B030301013), and the Shenzhen Key Laboratory of New Energy Resources Genome Preparation and Testing (No. ZDSYS201707281026184).

ABBREVIATIONS

LCO, LiCoO₂; RS, rock-salt; FP-LCO, coating LCO with F/P-containing species; LIBs, Li-ion batteries; CC, constant current; CV, constant voltage; CEI, cathode/electrolyte interface; EIS, electrochemical impedance spectroscopy; GITT, galvanostatic intermittent titration technique; TEM, transmission electron microscope; XRD, X-ray diffraction; XPS, X-ray photoelectron spectroscopy

REFERENCES

- (1) Liang, Z.; Wang, G.; Zeng, G.; Zhang, J.; Tang, Z. Highly Controlled Structured Catalysts for On-board Methanol Reforming. *J. Energy Chem.* **2022**, *68*, 19–26.
- (2) Lin, C.; Li, J.; Yin, Z. W.; Huang, W.; Zhao, Q.; Weng, Q.; Liu, Q.; Sun, J.; Chen, G.; Pan, F. Structural Understanding for High-Voltage Stabilization of Lithium Cobalt Oxide. *Adv. Mater.* **2024**, *36* (6), 2307404.
- (3) Ren, H.; Zhao, W.; Yi, H.; Chen, Z.; Ji, H.; Jun, Q.; Ding, W.; Li, Z.; Shang, M.; Fang, J.; et al. One-Step Sintering Synthesis Achieving Multiple Structure Modulations for High-Voltage LiCoO₂. *Adv. Funct. Mater.* **2023**, 33 (38), 2302622.
- (4) Yi, H.; Du, Y.; Fang, J.; Li, Z.; Ren, H.; Zhao, W.; Chen, H.; Zhou, L.; Zhao, Q.; Pan, F. Revealing the Grain-Boundary-Cracking Induced Capacity Decay of a High-Voltage LiCoO₂ at 4.6 V. ACS Appl. Mater. Interfaces 2023, 15 (36), 42667–42675.
- (5) Li, Z.; Yi, H.; Ren, H.; Fang, J.; Du, Y.; Zhao, W.; Chen, H.; Zhao, Q.; Pan, F. Multiple Surface Optimizations for a Highly Durable LiCoO₂ beyond 4.6 V. Adv. Funct. Mater. **2023**, 33 (46), 2307913.
- (6) Li, J.; Lin, C.; Weng, M.; Qiu, Y.; Chen, P.; Yang, K.; Huang, W.; Hong, Y.; Li, J.; Zhang, M.; et al. Structural Origin of the High-voltage Instability of Lithium Cobalt Oxide. *Nat. Nanotechnol.* **2021**, *16* (5), 599–605.
- (7) Lyu, Y.; Wu, X.; Wang, K.; Feng, Z.; Cheng, T.; Liu, Y.; Wang, M.; Chen, R.; Xu, L.; Zhou, J.; et al. An Overview on the Advances of $LiCoO_2$ Cathodes for Lithium-Ion Batteries. *Adv. Energy Mater.* **2021**, 11 (2), 2000982.
- (8) Wang, Q.; Yao, Z.; Wang, J.; Guo, H.; Li, C.; Zhou, D.; Bai, X.; Li, H.; Li, B.; Wagemaker, M.; et al. Chemical Short-range Disorder in Lithium Oxide Cathodes. *Nature* **2024**, *629* (8011), 341–347.
- (9) Huang, W.; Li, J.; Zhao, Q.; Li, S.; Ge, M.; Fang, J.; Chen, Z.; Yu, L.; Huang, X.; Zhao, W.; et al. Mechanochemically Robust LiCoO₂ with Ultrahigh Capacity and Prolonged Cyclability. *Adv. Mater.* **2024**, 36 (32), 2405519.
- (10) Zhang, Y.; Kim, J. C.; Song, H. W.; Lee, S. Recent Achievements Toward the Development of Ni-based Layered Oxide Cathodes for Fast-charging Li-ion Batteries. *Nanoscale* **2023**, *15* (9), 4195–4218.
- (11) Zhu, G. L.; Zhao, C. Z.; Huang, J. Q.; He, C.; Zhang, J.; Chen, S.; Xu, L.; Yuan, H.; Zhang, Q. Fast Charging Lithium Batteries: Recent Progress and Future Prospects. *Small* **2019**, *15* (15), 1805389.
- (12) Weiss, M.; Ruess, R.; Kasnatscheew, J.; Levartovsky, Y.; Levy, N. R.; Minnmann, P.; Stolz, L.; Waldmann, T.; Wohlfahrt-Mehrens, M.; Aurbach, D.; et al. Fast Charging of Lithium-Ion Batteries: A Review of Materials Aspects. *Adv. Energy Mater.* **2021**, *11* (33), 2101126.
- (13) Liu, Y.; Zhu, Y.; Cui, Y. Challenges and Opportunities Towards Fast-charging Battery Materials. *Nat. Energy* **2019**, *4* (7), 540–550.
- (14) He, J.; Meng, J.; Huang, Y. Challenges and Recent Progress in Fast-charging Lithium-ion Battery Materials. *J. Power Sources* **2023**, 570, 232965.
- (15) Huang, W.; Ye, Y.; Chen, H.; Vila, R. A.; Xiang, A.; Wang, H.; Liu, F.; Yu, Z.; Xu, J.; Zhang, Z.; et al. Onboard Early Detection and Mitigation of Lithium Plating in Fast-charging Batteries. *Nat. Commun.* 2022, 13 (1), 7091.
- (16) Weng, S.; Yang, G.; Zhang, S.; Liu, X.; Zhang, X.; Liu, Z.; Cao, M.; Ates, M. N.; Li, Y.; Chen, L.; et al. Kinetic Limits of Graphite Anode for Fast-Charging Lithium-Ion Batteries. *Nano-Micro Lett.* **2023**, *15* (1), 215.
- (17) Yao, Y. X.; Chen, X.; Yao, N.; Gao, J. H.; Xu, G.; Ding, J. F.; Song, C. L.; Cai, W. L.; Yan, C.; Zhang, Q. Unlocking Charge Transfer Limitations for Extreme Fast Charging of Li-Ion Batteries. *Angew. Chem., Int. Ed.* **2023**, *62* (4), No. e202214828.
- (18) Zou, Y.; Ma, Z.; Liu, G.; Li, Q.; Yin, D.; Shi, X.; Cao, Z.; Tian, Z.; Kim, H.; Guo, Y.; et al. Non-Flammable Electrolyte Enables High-Voltage and Wide-Temperature Lithium-Ion Batteries with Fast Charging. *Angew. Chem., Int. Ed.* **2023**, *62* (8), No. e202216189.

- (19) Kautz, D. J.; Cao, X.; Gao, P.; Matthews, B. E.; Xu, Y.; Han, K. S.; Omenya, F.; Engelhard, M. H.; Jia, H.; Wang, C.; et al. Designing Electrolytes With Controlled Solvation Structure for Fast-Charging Lithium-Ion Batteries. *Adv. Energy Mater.* **2023**, *13* (35), 2301199.
- (20) Zhang, X.; Zou, L.; Xu, Y.; Cao, X.; Engelhard, M. H.; Matthews, B. E.; Zhong, L.; Wu, H.; Jia, H.; Ren, X.; et al. Advanced Electrolytes for Fast-Charging High-Voltage Lithium-Ion Batteries in Wide-Temperature Range. *Adv. Energy Mater.* **2020**, *10* (22), 2000368.
- (21) Mo, Y.; Liu, G.; Yin, Y.; Tao, M.; Chen, J.; Peng, Y.; Wang, Y.; Yang, Y.; Wang, C.; Dong, X.; et al. Fluorinated Solvent Molecule Tuning Enables Fast-Charging and Low-Temperature Lithium-Ion Batteries. *Adv. Energy Mater.* **2023**, *13* (32), 2301285.
- (22) Roy, B.; Pal, U.; Simondson, D.; Nguyen, C.; Kerr, B. V.; Hocking, R. K.; Al-Masri, D.; Howlett, P. C.; Forsyth, M.; Kar, M.; et al. Extreme Fast Charging and Stable Cycling of Lithium Manganese Oxide Batteries by Suppression of Cathode Phase Changes. Adv. Funct. Mater. 2025, 35 (11), 2417317.
- (23) Kim, S.; Park, S.; Kim, M.; Cho, Y.; Kang, G.; Ko, S.; Yoon, D.; Hong, S.; Choi, N.-S. Improving Fast-Charging Performance of Lithium-Ion Batteries through Electrode–Electrolyte Interfacial Engineering. *Adv. Sci* **2025**, *12* (3), 2411466.
- (24) Tu, S.; Zhang, B.; Zhang, Y.; Chen, Z.; Wang, X.; Zhan, R.; Ou, Y.; Wang, W.; Liu, X.; Duan, X.; et al. Fast-charging Capability of Graphite-based Lithium-ion Batteries Enabled by Li₃P- Based Crystalline Solid—electrolyte Interphase. *Nat. Energy* **2023**, 8 (12), 1365–1374.
- (25) Zeng, W.; Xia, F.; Wang, J.; Yang, J.; Peng, H.; Shu, W.; Li, Q.; Wang, H.; Wang, G.; Mu, S.; et al. Entropy-increased LiMn₂O₄-based Positive Electrodes for Fast-charging Lithium Metal Batteries. *Nat. Commun.* **2024**, *15* (1), 7371.
- (26) Yan, S.; Chen, X.; Zhou, P.; Wang, P.; Zhou, H.; Zhang, W.; Xia, Y.; Liu, K. Regulating the Growth of Lithium Dendrite by Coating an Ultra-thin Layer of Gold on Separator for Improving the Fast-charging Ability of Graphite Anode. *J. Energy Chem.* **2022**, *67*, 467–473.
- (27) Zeng, Y.; Zhang, B.; Fu, Y.; Shen, F.; Zheng, Q.; Chalise, D.; Miao, R.; Kaur, S.; Lubner, S. D.; Tucker, M. C.; et al. Extreme Fast charging of Commercial Li-ion Batteries via Combined Thermal Switching and Self-heating Approaches. *Nat. Commun.* **2023**, *14* (1), 2220
- (28) Ku, K.; Son, S.-B.; Gim, J.; Park, J.; Liang, Y.; Stark, A.; Lee, E.; Libera, J. Understanding the Constant-voltage Fast-charging Process Using a High-rate Ni-rich Cathode Material for Lithium-ion Batteries. *J. Mater. Chem. A* **2021**, *10* (1), 288–295.
- (29) Zhu, Y.; Wu, D.; Yang, X.; Zeng, L.; Zhang, J.; Chen, D.; Wang, B.; Gu, M. Microscopic Investigation of Crack and Strain of LiCoO₂ Cathode Cycled Under High Voltage. *Energy Storage Mater.* **2023**, *60*, 102828.
- (30) Park, N. Y.; Kim, M. C.; Han, S. M.; Park, G. T.; Kim, D. H.; Kim, M. S.; Sun, Y. K. Mechanism Behind the Loss of Fast Charging Capability in Nickel-Rich Cathode Materials. *Angew. Chem., Int. Ed.* **2024**, *63* (12), No. e202319707.
- (31) Yu, L.; Huang, Y.; Han, Q.; Zhu, J.; Lu, J. High Cycling Rate-Induced Irreversible TMO_6 Slabs Glide in Co-Free High-Ni Layered Cathode Materials. *Adv. Funct. Mater.* **2023**, 33 (32), 2301650.
- (32) Hu, J.; Fan, F.; Zhang, Q.; Zhong, S.; Ma, Q. Effects of Long-term Fast Charging on a Layered Cathode for Lithium-ion Batteries. *J. Energy Chem.* **2022**, *67*, 604–612.
- (33) Yang, Y.; Xu, R.; Zhang, K.; Lee, S. -J.; Mu, L.; Liu, P.; Waters, C. K.; Spence, S.; Xu, Z.; Wei, C.; et al. Quantification of Heterogeneous Degradation in Li-Ion Batteries. *Adv. Energy Mater.* **2019**, 9 (25), 1900674.
- (34) Park, J.; Zhao, H.; Kang, S. D.; Lim, K.; Chen, C. C.; Yu, Y. S.; Braatz, R. D.; Shapiro, D. A.; Hong, J.; Toney, M. F.; et al. Fictitious Phase Separation in Li Layered Oxides Driven by Electroautocatalysis. *Nat. Mater.* **2021**, 20 (7), 991–999.
- (35) Xia, S.; Mu, L.; Xu, Z.; Wang, J.; Wei, C.; Liu, L.; Pianetta, P.; Zhao, K.; Yu, X.; Lin, F.; et al. Chemomechanical Interplay of Layered

- Cathode Materials Undergoing Fast Charging in Lithium Batteries. Nano Energy 2018, 53, 753-762.
- (36) Meng, D.; Xue, Z.; Chen, G.; Zhou, D.; He, Y.-S.; Ma, Z.-F.; Liu, Y.; Li, L. Multiscale Correlative Imaging Reveals Sequential and Heterogeneous Degradations in Fast-charging Batteries. Energy Environ. Sci. 2024, 17 (13), 4658-4669.
- (37) Sieg, J.; Schmid, A. U.; Rau, L.; Gesterkamp, A.; Storch, M.; Spier, B.; Birke, K. P.; Sauer, D. U. Fast-charging Capability of Lithium-ion Cells: Influence of Electrode Aging and Electrolyte Consumption. Appl. Energy 2022, 305, 117747.
- (38) Bi, Z.; Yi, Z.; Zhang, L.; Wang, G.; Zhang, A.; Liao, S.; Zhao, Q.; Peng, Z.; Song, L.; Wang, Y.; et al. Ultrathin Dense LiF Coverage Coupled with a Near-surface Gradient Fluorination Lattice Enables Fast-charging Long-life 4.6 V LiCoO₂. Energy Environ. Sci. 2024, 17 (8), 2765-2775.
- (39) Wang, X.; Ren, H.; Du, Y.; Li, Z.; Zhao, W.; Ji, H.; Yi, H.; Pan, Q.; Liu, J.; Lou, Z.; et al. Tuning Surface Chemistry to Reduce the Step-like Degradation of LiCoO₂ at 4.6 V. Nano Energy 2024, 125, 109537.
- (40) Zhu, M.; Huang, Y.; Chen, G.; Lu, M.; Nevar, A. A.; Dudko, N.; Shi, L.; Huang, L.; Tarasenko, N.V.; Zhang, D. Sn, S co-doped LiCoO2 with Low Lithium Ion Diffusion Energy Barrier and High Passivation Surface for Fast Charging Lithium ion Batteries. Chem. Eng. J. 2023, 468, 143585.
- (41) Qin, R.; Ding, S.; Hou, C.; Liu, L.; Wang, Y.; Zhao, W.; Yao, L.; Shao, Y.; Zou, R.; Zhao, Q.; et al. Modulating the Proton-Conducting Lanes in Spinel ZnMn₂O₄ through Off-Stoichiometry. Adv. Energy Mater. 2023, 13 (20), 2203915.
- (42) Ye, Y.; Xu, R.; Huang, W.; Ai, H.; Zhang, W.; Affeld, J. O.; Cui, A.; Liu, F.; Gao, X.; Chen, Z.; et al. Quadruple the Rate Capability of High-energy Batteries Through a Porous Current Collector Design. Nat. Energy 2024, 9 (6), 643-653.
- (43) Li, J.; Sharma, N.; Jiang, Z.; Yang, Y.; Monaco, F.; Xu, Z.; Hou, D.; Ratner, D.; Pianetta, P.; Cloetens, P.; et al. Dynamics of Particle Network in Composite Battery Cathodes. Science 2022, 376 (6592), 517-521.
- (44) Li, Z.; Yi, H.; Ding, W.; Ren, H.; Du, Y.; Shang, M.; Zhao, W.; Chen, H.; Zhou, L.; Lin, H.; et al. Revealing the Accelerated Capacity Decay of a High-Voltage LiCoO₂ upon Harsh Charging Procedure. Adv. Funct. Mater. 2024, 34 (14), 2312837.
- (45) Zhao, Q.; Song, A.; Zhao, W.; Qin, R.; Ding, S.; Chen, X.; Song, Y.; Yang, L.; Lin, H.; Li, S.; et al. Boosting the Energy Density of Aqueous Batteries via Facile Grotthuss Proton Transport. Angew. Chem., Int. Ed. 2021, 60 (8), 4169-4174.
- (46) Verdier, S.; El Ouatani, L.; Dedryvère, R.; Bonhomme, F.; Biensan, P.; Gonbeau, D. XPS Study on Al₂O₃- and AlPO₄- Coated LiCoO₂ Cathode Material for High-Capacity Li Ion Batteries. J. Electrochem. Soc. 2007, 154 (12), A1088.
- (47) Ding, W.; Ren, H.; Li, Z.; Shang, M.; Song, Y.; Zhao, W.; Chang, L.; Pang, T.; Xu, S.; Yi, H.; et al. Tuning Surface Rock-Salt Layer as Effective O Capture for Enhanced Structure Durability of LiCoO₂ at 4.65 V. Adv. Energy Mater. **2024**, 14 (13), 2303926.
- (48) Shang, M.; Ren, H.; Zhao, W.; Li, Z.; Fang, J.; Chen, H.; Fan, W.; Pan, F.; Zhao, Q. Alleviating Structure Collapse of Polycrystalline LiNi_xCo_yMn_{1-x-y}O₂ via Surface Co Enrichment. ACS Nano **2024**, 18 (26), 16982-16993.

